

# Study the build-up, initiation and acceleration of 2008 April 26 coronal mass ejection observed by STEREO

X. Cheng<sup>1,2</sup>, M. D. Ding<sup>1,2</sup> and J. Zhang<sup>3,1</sup>

Received \_\_\_\_\_; accepted \_\_\_\_\_

---

<sup>1</sup>Department of Astronomy, Nanjing University, Nanjing, 210093, China;  
dmd@nju.edu.cn

<sup>2</sup>Key Laboratory of Modern Astronomy and Astrophysics (Ministry of Education), Nanjing University, Nanjing 210093, China

<sup>3</sup>Department of Computational and Data Sciences, George Mason University, 4400 University Drive, MSN 6A2, Fairfax, VA 22030

## ABSTRACT

In this paper, we analyze the full evolution, from a few days prior to the eruption to the initiation, and the final acceleration and propagation, of the CME that occurred on 2008 April 26 using the unprecedented high cadence and multi-wavelength observations by STEREO. There existed frequent filament activities and EUV jets prior to the CME eruption for a few days. These activities were probably caused by the magnetic reconnection in the lower atmosphere driven by photospheric convergence motions, which were evident in the sequence of magnetogram images from MDI (Michelson Doppler Imager) onboard SOHO. The slow low-layer magnetic reconnection may be responsible for the storage of magnetic free energy in the corona and the formation of a sigmoidal core field or a flux rope leading to the eventual eruption. The occurrence of EUV brightenings in the sigmoidal core field prior to the rise of the flux rope implies that the eruption was triggered by the inner tether-cutting reconnection, but not the external breakout reconnection. During the period of impulsive acceleration, the time profile of the CME acceleration in the inner corona is found to be consistent with the time profile of the reconnection electric field inferred from the footpoint separation and the RHESSI 15-25 keV HXR flux curve of the associated flare. The full evolution of this CME can be described in four distinct phases: the build-up phase, initiation phase, main acceleration phase, and propagation phase. The physical properties and the transition between these phases are discussed, in an attempt to provide a global picture of CME dynamic evolution.

*Subject headings:* Sun: corona — Sun: coronal mass ejections (CMEs) — Sun: flares — Sun: magnetic fields

## 1. Introduction

Coronal mass ejections (CMEs) are large-scale activities releasing a vast amount of plasma and solar energetic particles (SEPs) into the outer space (Gosling et al. 1993; Webb et al. 1994). These plasma and SEPs can propagate into the magnetosphere near the Earth and severely affect space-based modern technological systems, especially during the solar maximum (Smart & Shea 1989). Solar physicists have been pursuing what happens prior to the CME initiation and how CMEs are initiated. Various observational signatures, including magnetic cancellation, magnetic flux emergence, sigmoids, and filament activities are regarded as the significant precursors of CME eruptions (Martin 1998; Canfield et al. 2000; Wang 2006; Gibson et al. 2006). The common nature of these signatures are magnetic free energy build-up in the corona. As a consequence of the energy build-up, the coronal magnetic fields may explosively erupt once a trigger leads to the loss of equilibrium (Forbes et al. 2006). However, there is no consensus so far on the exact trigger mechanism. The MHD instability model suggests that the eruption of CMEs that have a flux rope morphology is probably caused by the kink and/or torus instability when the winding of the field lines exceeds a critical value (Sturrock et al. 2001; Linker et al. 2001; Fan et al. 2004; Rust et al. 2005; Török & Kliem 2005; Gibson et al. 2006). In the tether-cutting model, the magnetic reconnection that occurs close to the polarity inversion line plays the role of weakening the constraining tension force of the overlying field, and results in the rise of the sigmoid-shaped core field and subsequently the runaway eruption (Moore & Labonte 1980; Moore et al. 2001; Sturrock et al. 1989; Liu et al. 2007; Sterling et al. 2007). The same tension reduction mechanism holds for the flux emergence model suggested by Chen et al. (2000) in which the magnetic reconnection occurs between the emerging field and the background field. In the breakout model proposed by Antiochos et al. (1999), the overlying magnetic field constraining the sheared core field is removed through external magnetic reconnection, which leads to the CME eruption. Other authors have proposed that the

injection of poloidal magnetic flux (of sub-photospheric origin) in the flux rope can cause a CME to take off (Chen et al. 2000, 2003; Krall et al. 2001). More details about CME initiation mechanisms can be found in the reviews (e.g., Forbes 2000, 2006; Gopalswamy 2003; Chen 2008; Schrijver 2009).

One key aspect of understanding CME eruption is of understanding the relationship between CMEs and flares, which itself has been a long-standing elusive issue for decades (Kahler 1992; Gosling et al. 1993; Hundhausen 1999). Zhang et al. (2001, 2004) proposed three phases of CME kinematic evolution: the initiation phase, impulsive acceleration phase, and propagation phase, which are tightly associated with the three phases of the associated flare: the pre-flare phase, flare rise phase, and flare decay phase, respectively (see also, Burkepile et al. 2004; Vršnak et al. 2005b). The temporal correlation between CME acceleration and flare HXR flux was studied by Qiu et al. (2004) and Temmer et al. (2008). In the standard CME-flare model, the flare ribbons separate in the chromosphere during the CME impulsive acceleration phase because of continuous magnetic field reconnection. The reconnection rate can be calculated in terms of flare ribbon separation speed and the line-of-sight component of magnetic fields (Forbes & Priest 1984; Poletto & Kopp 1986; Forbes & Lin 2000; Qiu et al. 2002). Qiu et al. (2004) compared the reconnection rate with the acceleration of the filament/CME and found a similarity between them. It was also found that the total reconnection flux is proportional to the maximum speed of CMEs (e.g., Qiu et al. 2005). In addition, Liu et al. (2009) found that the spectral index of X-ray emission of flares is strongly anti-correlated with the reconnection electric field. All of these suggest that CMEs and the associated flares, during the impulsive energy-release phase in particular, are driven by the same physical process in the lower corona, presumably via magnetic reconnection (Lin et al. 2000; Priest et al. 2002; Vršnak et al. 2004; Zhang et al. 2006; Maričić et al. 2007; Temmer et al. 2008).

As a matter of fact, most previous studies concerning CMEs address only certain specific phases of CME evolution, while very few are for the full evolution cycle from the build-up phase (tens of hours prior to the CME initiation), throughout the initiation phase and acceleration phase, and to the propagation phase. Therefore, it is useful to make a complete observation to investigate the full CME evolution. It is also of particular interest to study the variation of magnetic topology involved in different evolution phases, which shall shed light on possible initiation mechanisms of CMEs. The unique data of high cadence and full coverage acquired by SECCHI (Sun Earth Connection Coronal and Heliospheric Investigation; Howard et al. 2008) instruments onboard STEREO (Solar Terrestrial Relations Observatory; Kaiser et al. 2008) spacecraft provide us the opportunity to make such a study. In this paper, we investigate the full evolution of the CME on 2008 April 26 which was well observed by STEREO. In §2, we describe the instruments and the data. Our analysis and results are shown in §3 and §4. In §5, a schematic model is proposed to explain the full evolution of the CME, followed by discussions and conclusions in §6.

## 2. Instruments and Observations

The STEREO spacecraft were designed to monitor solar activities from two different perspectives in space, which for the first time provide the stereoscopic measurement for understanding solar eruptions. STEREO A moves ahead of the earth in its orbit and STEREO B trails behind. The separation between the two spacecraft has been continuously increasing. In particular, the separation angle was  $49^{\circ}.5$  on 2008 April 26 so that the CME studied in this paper were observed from two well-separated perspectives.

The SECCHI instrument suite on board STEREO is composed of five telescopes. Most of the data analyzed in this paper are from three of them: Extreme UltraViolet Imager (EUVI), Inner Coronagraph (COR1), and Outer Coronagraph (COR2). EUVI

observes solar chromosphere and the lower corona at four passbands: 171 Å, 195 Å, 284 Å, and 304 Å, with a cadence higher than EIT (Extreme-ultraviolet Imaging Telescope; Delaboudinière et al. 1995) onboard SOHO, especially at 171 Å passband. COR1 and COR2 are externally occulted white-light coronagraphs with fields of view (FOVs) of  $1.4\text{--}4.0R_{\odot}$  and  $2.5\text{--}15.6R_{\odot}$ , respectively. Both of them have a cadence higher than LASCO (Large Angle and Spectrometric Coronagraph; Brueckner et al. 1995) on board SOHO. Therefore, the SECCHI instruments can well observe CMEs from its birth place on the solar surface to its ultimate propagation in the outer corona.

In addition, GOES X-ray data reveal the temporal profile of the soft X-ray emission at 1–8 Å for solar-flares, which are often associated with CMEs. The RHESSI (Reuven Ramaty High Energy Solar Spectroscopic Imager; Lin et al. 2002) spacecraft provides the HXR light curve of the flares. The location of flares can be found in Solar Geophysics Data Reports<sup>1</sup>. The MDI (Michelson Doppler Imager; Scherrer et al. 1995) images provides the longitudinal magnetic field at the surface of the Sun.

Up to date, more than three hundred CMEs have been observed by STEREO since the launch in 2006 December<sup>2</sup>. The CME that occurred on 2008 April 26 was associated with a GOES B3.8 class flare. It appeared near the solar limb as seen from the perspective of STEREO A while near the disk center as a halo CME as seen from the perspective of STEREO B. From inspecting the running difference images, the leading edge (LE) of the CME that appeared in the FOVs of COR1 and COR2 was evidently sharp, thus in favor of the height measurement. From the height measurement, we can further infer the CME’s kinematical evolution. Recently, Thernisien et al. (2009) obtained its 3D velocity and average acceleration by a forward modeling method using only the SECCHI/COR2

---

<sup>1</sup><http://www.ngdc.noaa.gov/stp/SOLAR>

<sup>2</sup><http://cor1.gsfc.nasa.gov/>

observations. Here, we study this event using multi-wavelength data with a focus on its full evolution, including the magnetic topology in different phases.

### 3. Precursors, Initiation, and Eruption of the CME

#### 3.1. Magnetic Cancellation in the Active Region

Inspecting the surface source region in magnetogram images, we found a continuous flux cancellation for several days prior to the eruption. We plotted in Figure 1 the line-of-sight (LOS) magnetic field of the active region in which the CME was originated. The three magnetograms in Figure 1 were taken in three consecutive days prior to the CME eruption; they had been rotated to the same time in order to have a better comparative view. The cancellation of magnetic flux mainly occurred near the polarity inversion line (PIL). We showed in Figure 2 the changes of the magnetic fluxes in both the whole region (left panel) and the central region (indicated by the white rectangle in Figure 1). Both the positive flux and the negative flux decreased slowly, as well as the unsigned magnetic flux in the whole region. For the central region near the PIL, the positive magnetic flux decreased sharply from about  $5.8 \times 10^{20}$  to  $2.2 \times 10^{20}$  Mx during the three days before the eruption. Note that the increasing of negative magnetic flux for about one day prior to the onset of the CME/flare (denoted by the vertical solid line in Figure 2), was due to the motion of the negative patch toward the northeast; the change was caused by flux transportation instead of flux emergence. Therefore, the slow converging motion between the two opposite polarities, driven probably by photospheric flows, resulted in the continuous magnetic cancellation. We believe that this photospheric flux cancellation process lead to subsequent filament activities and ultimately the CME we will be discussing. The magnetic cancellation has been considered as one of primary magnetic signatures leading to major solar activities (e.g., Wang et al. 2006).

### 3.2. Disappearance of the Associated Filaments

We carefully examined what occurred in the corona of the source active region within two days prior to the CME eruption. As shown in the left and middle panels of Figure 3, there appeared the existence of a filament over the active region. It was initially visible for several hours on April 24, during which several jets occurred, indicated by the white arrow in the left panel. The filament was also visible on April 25 during which some mass flew down slowly along the field lines. Eventually, the filament rose impulsively on April 26 (indicated by the white arrow in the right panel of Figure 3). Note that such active behaviors of filaments before their final eruption has been well observed before (see the review by Pick et al. 2006). Nevertheless, the final eruption of filaments is closely associated with that of CMEs.

### 3.3. Sigmoid Configuration and EUV Brightening

The CME of interest also had the sigmoid signature prior to the eruption. Figure 4 showed some sampling EUV images of the active region prior to the CME eruption; the sigmoid was particularly obvious in the 284 Å (lower-middle panel) and 195 Å (lower-right) passband images. The 171 Å passband images, on the other hand, did not show the sigmoid well, but revealed better the morphology of the overlying magnetic loop arcade (upper panels). The sigmoid seemed consisting of two co-existing J-shaped bundles of low-lying loops forming a reversed-S shape in projection; the two ends were in opposite sides of the PIL and anti-parallel to each other. Similar sigmoid structures comprising of many individual loops have been identified by McKenzie et al. (2008). Such structures are preferentially observed in eruption regions and thus have been regarded as a precursor of CMEs (Canfield et al. 2000; Gibson et al. 2006). Note that, the 195 Å image at 9:06 UT on April 25 (lower-left panel) showed the coronal configuration prior to the formation of the



coronal sigmoid.

Another noticeable feature was the EUV brightening in the sigmoid core field, most clearly seen in the 171 Å passband images, as denoted by the two small squares in Figure 4 (upper panels). The brightening can also be seen in the 284 and 195 Å passband images. Such brightening, first appearing at  $\sim 12:40$  UT, implies that magnetic reconnection occurred at this site about one hour before the eruption. We also note that some twisted field lines in the sigmoid started to rise slowly from  $\sim 13:36$  UT. These observations help understand the triggering or initiation mechanism of the CME. They seem to favor the tether cutting model proposed by Moore et al (2001) and further elaborated by Liu (2007), but not the breakout model proposed by Antiochos et al. (1999). First, the active region on the photosphere appeared as a simple bipolar magnetic field, and the corona magnetic field could be characterized by a sigmoidal core field constraining by an overlying bipolar arcade field. Secondly, the pre-eruption EUV brightenings only occurred within the core field; we do not find any remote brightenings surrounding the active region as expected from the breakout model (Moore & Sterling 2006). The breakout model usually requires a quadrupole magnetic configuration and an initiation magnetic reconnection at the null point above the central core field. Therefore, the observational features of this event are well consistent with the tether-cutting model, in which the magnetic reconnection occurs within the low-lying core field lines (Moore et al. 2001). We believe that the initial reconnection, as indicated by the EUV brightenings, caused the slow rise of the sigmoidal magnetic structure.

### 3.4. Eruption of the CME

From inspecting the EUVI movies, we found that the overlying field lines were relatively stable for days before the eruption at about 13:44 UT, at which the whole system

became unstable and erupted impulsively. The CME first appeared in the FOV of the COR1 A image at 14:15 UT at a height of  $1.91R_{\odot}$  from the disk center. From the COR1 A movie, one can clearly see that a sharp semicircular front expanded outward. Whereas, the CME first appeared in the FOV of the COR1 B image at 14:25 UT as a halo shape at a height of  $1.72R_{\odot}$ . At 14:55 UT, another inner halo structure appeared. The two halos may correspond to the CME disturbance front and the expanding flux rope, respectively (see also, Wood & Howard 2009). Selected snapshots of the CME were shown in Figure 5. Note that during the CME eruption, a streamer disturbance was triggered at the southern side as indicated by the black arrow in Figure 5.

#### 4. Kinematics of the CME

We can well track the LE of the CME using the running difference images at  $171 \text{ \AA}$  and in white light images, as shown in Figure 5. The white arrows in the figure pointed to the position angle of the measurement, at which we measured the height-time variation of the CME. The height-time measurement was then used to derive the velocity profile through the piece-wise numerical derivative method, i.e., the Lagrangian interpolation of three neighboring points (Zhang et al. 2001, 2004). From the velocity profile, the CME acceleration can be further derived through a similar method but having a larger uncertainty. We thus obtained the full kinematic evolution of the event from the solar surface continuously to the outer corona as indicated in the middle panels of Figure 7. Note that the uncertainty in the height measurements was estimated to be 0.026, 0.12, and  $0.24 R_{\odot}$  for EUVI, COR1, and COR2, respectively. This is the main factor causing the uncertainty in the calculation of speed and acceleration of a CME (Zhang et al. 2004).

The reconnection electric field can be calculated using the separation speed of the  $H\alpha$  ribbons, serving as a proxy of the magnetic reconnection rate. Here, we revisited this issue

using EUVI observations. For the event here, the flare ribbons were well shaped and thus can be easily traced. We chose five directions, marked by the white lines in Figure 6, to measure the separation speed of the flare ribbons. The final separation speed was obtained by average the speeds along the five lines. The magnetic field was taken from the MDI magnetogram image just prior to the CME eruption. Since the event occurred near the disk center as seen from SOHO, the observed LOS magnetic field should be close to the radial component of the fields needed for the calculation. The reconnection electric field can then be inferred as  $E_{rec} = \overline{V}B_n$ , which was plotted as the green lines in the bottom panels of Figure 7.

The relationship between the acceleration phase of the CME and the impulsive phase of the associated flare had been investigated in many papers (e.g., Zhang et al. 2001, 2004, Temmer et al. 2008). Qiu et al. (2004) and Jing et al. (2005) compared in detail the acceleration of the CME, the reconnection rate, and the HXR emission of the associated flare. In the two studies, they used the filament acceleration as the proxy of CME acceleration because of the lack of CME observations in the inner corona. However, thanks to the STEREO observations, we were able to study the event on 2008 April 26 with better continuity in space and time. We derived the CME’s acceleration from two well-separated viewing angles and tracked the CME continuously from the solar surface to the outer corona. We then compared the CME’ acceleration with the reconnection rate and the HXR flux of the associated flare, as shown in the bottom panels of Figure 7. The acceleration of the CME peaked at 13:51 UT, while the reconnection electric field and the RHESSI 15–25 keV HXR flux peaked at 13:54 UT. This time difference was relatively small and was within the time resolution of the CME acceleration curve. In general, the profile of CME acceleration was coincident with the profile of the reconnection electric field and the HXR flux curve.

## 5. A Four-Phase CME Evolution Model

In this section, we attempt to use a schematic model to explain the full evolution of the CME from the early development to the ultimate eruption (Figure 8). We piece together many components proposed by other researchers which we believe were relevant to CME evolution and put them into a coherent scenario. For the sake of clarity of discussion, we suggest that the full evolution of the CME should be divided into four phases: (1) the build-up phase, (2) the initiation phase, (3) the main acceleration phase, and (4) the propagation phase.

The build-up phase was the phase of preparation that lasted for days. As discussed earlier, it was characterized by many pre-cursor signatures: flux cancellation, filament activity, sigmoid and EUV brightening, even though these signatures were neither necessary nor sufficient for an eruption. Formation and evolution of filaments had been extensively studied for many years. Martens et al. (2001) proposed a head-to-tail model to explain the formation of filaments through flux convergence and cancellation. Subsequently, Welsch et al. (2005) simulated the filament formation using two flux systems driven by the convergence of opposite polarities along PILs. Chae et al. (2001) proposed that slow magnetic reconnection last all the time in the chromosphere driven by converging motions. The continuous reconnection can result in both the overlying field lines straddling the neutral line and the low-lying core field lines (Chae et al. 2001; Welsch et al. 2005).

Further, some EUV jets and small eruptions took place at the site of magnetic cancellation. As the positive and negative fluxes moved close to each other near the PIL, the anti-parallel inner ends of the two bundles of the loops reconnected slowly and continuously in the lower atmosphere (i.e., the chromosphere). That resulted in the formation of the overlying M-shaped field lines, almost perpendicular to the PIL. At the same time, it also produced the low-lying field lines, near parallel with the PIL. The active filaments were

condensed at the dip of the M-shaped field lines, as indicated in the upper right panel of Figure 8. As the filament mass flew down along the M-shaped field lines, more field lines rose and served as the overlying loops. These loops were heated slowly and remained to be invisible at  $171 \text{ \AA}$  until about tens of hours prior to the CME eruption. Note that, as long as some open field lines exist at the reconnection site, part of the filament mass may erupt as EUV jets. However, although part of the filament mass flew down slowly or erupted, the rest of the filament appeared to be quite stable in the dip of the field lines all the time prior to the CME eruption (Figure 8c). With time going on, the lower field lines in the eastern part and the pre-existing field lines in the western part, being both J-shaped, moved closer to each other, driven by the continuous convergence motion along the PIL and formed a reversed-S sigmoid structure in the projection plane. Then, the ends of the two bundles of the J-shaped loops, on the opposite sides of the PIL, reconnected as tether-cutting and formed the little twisted field lines, while the energy released through the reconnection heated the plasma in the middle part of the reversed-S sigmoid configuration and thus producing the observed EUV brightenings. The shortest field lines submerged into the sub-photosphere after the slow reconnection, which was manifested by the magnetic cancellation in the photosphere (Figure 8b–d). Recently, Tripathi et al. (2009) and Green & Kliem (2009) also reported such sigmoid structure coming into existence after a pair of J-shaped arcs reconnecting through flux cancellation in the photosphere. It should be noted that these sigmoid structures may provide observational evidence of the flux rope existence prior to the CME eruption, which was useful for distinguishing different CME-flare models.

The initiation phase occurred when the upward force within the sigmoid was able to overcome the tension force of the overlying field lines. As more and more J-shaped loops reconnected by tether-cutting, the twisted field lines in the reversed-S sigmoid configuration beneath the overlying loops moved up due to an increased upward magnetic hoop force and a decreased downward magnetic stress (Moore et al. 2001; Liu et al. 2007; Sterling et al.

2007). The rising twisted field lines pushed upward the overlying loops. When the overlying loops were stretched to a certain extent due to the tether cutting reconnection, a current sheet between the legs of the distended overlying field line was formed under the loops so that a fast runaway reconnection was subsequently initiated, leading to the main energy release phase and the impulsive acceleration of the CME; this is the standard model of eruptive flares (Hirayama 1974). Another possibility leading to the main eruption is the triggering of MHD instability of the flux rope formed from the tether cutting reconnection, through kink and/or torus instability (Török & Kliem 2005; Kliem & Török 2006).

The subsequent main acceleration phase is believed to be caused by the runaway magnetic reconnection, coupled with the explosive poloidal flux injection into the rising flux rope. The reconnection rapidly injected a large amount of poloidal flux into the twisted field lines, thus supplied a stronger upward driving force so as to impulsively accelerate the CME flux rope. On the other hand, the CME eruption led to a decrease of the magnetic pressure below the flux rope, which caused a faster inflow toward the current sheet and enhanced the runaway reconnection. This positive feedback process effectively released the magnetic free energy stored in the lower corona, which converted into the kinetic energy of the CME and also produced the enhanced soft X-ray and hard X-ray emissions (Li et al. 1993). Moreover, the CME eruption led to a depletion of mass in the lower atmosphere near the active region and formed the coronal dimming (Thompson et al. 1998). As the magnetic reconnection progressed, the reconnection site rose gradually. The upward moving reconnection site induced the flare ribbons to separate horizontally at the base of the corona, as evidently seen in the EUV and  $H\alpha$  channels. Beneath the reconnection site, the newly reconnected magnetic loops were filled by the plasma evaporated from the chromosphere and the sigmoid magnetic structure changed to post-flare loop arcades (see also, Liu et al. 2007), as shown in Figure 8f. Note that the magnetic configuration before the eruption (Figure 8c) had been unambiguously confirmed by the extrapolated coronal magnetic field obtained from a linear

force-free field (LFFF) model using the MDI magnetogram as the input.

After the main phase that lasted about 10 minutes, the runaway reconnection came to a stop. The CME now entered into the simple propagation phase: the CME was propagating in nearly a constant speed or with a small residual acceleration in the outer corona.

## 6. Discussions and Conclusions

The STEREO observations provide an unprecedented opportunity to investigate solar eruptions. In this paper, we presented multi-wavelength observations of the flare-associated CME that occurred on 2008 April 26. We had studied its evolution for a long period and discussed the full evolution in a four-phase scenario: the build-up phase, initiation phase, main acceleration phase, and propagation phase. During the build-up phase, the active filaments, instantaneous EUV jets, and a reversed-S sigmoid structure were observed. All the features were physically related to the persistent slow magnetic reconnection in the solar lower atmosphere, which was manifested as photospheric magnetic cancellation. Before the eruption, there was a long period of reconnection occurring in the lower layers resulting in the transferring and accumulation of magnetic free energy, as well as the formation of a magnetic structure favorable for eruption, i.e., the sigmoid structure in this event. Different from the process of flux cancellation, the emerging of magnetic flux may also play an important role in transferring magnetic free energy from the sub-photosphere into the corona (Tian et al. 2008; Archontis et al. 2009). MacNeice et al. (2004) showed that, as the magnetic field shear increases, the magnetic free energy is continuously accumulated. They also proposed that such a quasi-static energy accumulation phase is necessary for any fast CME eruption. The magnetic field shear can be caused by the convergence motion of opposite magnetic fluxes (Titov et al. 2008). Using a nonlinear force-free field extrapolation, it was recently found that the accumulated magnetic free energy increases

with time prior to the eruption (Thalmann & Wiegmann 2008; Guo et al. 2008; Jing et al. 2009). Therefore, the build-up phase accumulates the sufficient magnetic free energy for the eventual initiation and the final eruption.

In general, the initiation phase of a CME eruption is characterized by a slow rise of the CME flux rope. In the present event, the EUV emission started to brighten in the core part of the reversed-S sigmoid configuration, which implied that slow magnetic reconnection was taking place there. As the field lines in the reversed-S sigmoid configuration continually reconnected, the CME flux rope rose slowly for about 20 minutes. This inner core magnetic reconnection prior to the eruption, combined with the facts of the bipolar magnetic structure in the active region and the absence of remote brightenings, seems to rule out the breakout model as the triggering mechanism of this event. Instead, we think that this eruption is well consistent with the tether-cutting initiation model. We also investigated the kinematics of this CME and found that its acceleration was well correlated with the HXR flux of the associated flare and the magnetic reconnection rate (see also, Zhang et al. 2004; Qiu et al. 2004; Temmer et al. 2008). It suggests that the main acceleration phase of the CME in the inner corona is likely caused by the fast runaway magnetic reconnection. Later on, the CME propagated with almost a constant velocity in the outer corona (see also, Zhang et al. 2001, Gallagher et al. 2003). However, for CMEs associated with a long decay flare, even though the fast magnetic reconnection ceases, a positive post-impulsive-phase acceleration may continue to exist after the impulsive acceleration phase (Cheng et al. 2009). In general, these observational results are consistent with the standard CME-flare model.

We think that the schematic model that comprises of the four phases proposed in this paper can be applied to most CME events. However, owing to different physical circumstances under which CMEs occur, individual events may have their own characteristics. In particular, there may be various manifestations for the build-up phase



and the initiation phase, as mentioned above. We look forward to more observations in the coming years to study a variety of CME events, in order to fully understand the full evolution cycle of CMEs, including energy build-up, initiation, impulsive acceleration and subsequent propagation in the interplanetary space.

We thank to the referee for the valuable suggestions and comments that helped to improve the paper significantly. We are grateful to P. F. Chen, Z. J. Ning, and C. Liu for valuable discussions, and to M. Jin for help on data analysis. We thank the STEREO/SECCHI data provided by a consortium of NRL (US), LMSAL (US), NASA/GSFC (US), RAL (UK), UBHAM (UK), MPS (Germany), CSL (Belgium), IOTA (France), and IAS (France). This work was supported by NSFC under grants 10673004, 10828306, and 10933003 and NKBRSF under grant 2006CB806302. SOHO is a project of international cooperation between ESA and NASA.

## REFERENCES

- Antiochos, S. K., DeVore, C. R., & Klimchuk, J. A. 1999, *ApJ*, 510, 485
- Archontis, V., Hood, A. W., Savcheva, A., Golub, L., & Deluca, E. 2009, *ApJ*, 691, 1276
- Brueckner, G. E., et al. 1995, *Sol. Phys.*, 162, 357
- Burkepile, J. T., Hundhausen, A. J., Stanger, A. L., St.Cyr, O. C., & Seiden, J. A. 2004, *J. Geophys. Res.*, 109, A03103
- Canfield, R. C., Hudson, H. S., & Pevtsov, A. A. 2000, *IEEE Transactions on Plasma Science*, 28, 1786
- Chae, J., Wang, H. M., Qiu, J., Goode, P. R. Strous, L., & Yun, H. S. 2001, *ApJ*, 560, 476
- Chen, P. F., & Shibata, K. 2000, *ApJ*, 545, 524
- Chen, P. F. 2008, *Journal of Astrophysics and Astronomy*, 29, 179
- Chen, J., et al. 2000, *ApJ*, 533, 481
- Chen, J. & Krall, J. 2003, *J. Geophys. Res.*, 108(ALL), 1410(PaperI)
- Cheng, X., Zhang, J., Ding, M. D., & Spoomvises, W. 2010, *ApJ*, in press
- Delaboudinière, J. P., et al. 1995, *Sol. Phys.*, 162, 291
- Fan, Y., & Gibson, S. E. 2004, *ApJ*, 609, 1123
- Forbes, T. G., & Priest, E. R. 1984, in *Solar Terrestrial Physics: Present and Future*, ed. D. M. Butler and K. Paradupoulous (NASA), 1
- Forbes, T. G., & Lin, J. 2000, *J. Atmos. Sol-Terr. Phys.*, 62, 1449
- Forbes, T. G. 2000, *J. Geophys. Res.*, 105, 23153

- Forbes, T. G., et al. 2006, *Space Science Reviews*, 123, 251
- Gallagher, P. T., Lawrence, G. R., & Dennis, B. R. 2003, *ApJ*, 588, L53
- Gibson, S. E., & Fan, Y. 2006, *J. Geophys. Res.*, 111, A12103
- Gibson, S. E., Fan, Y., Török, T., & Kliem, B. 2006, *Space Science Reviews*, 124, 131
- Gopalswamy, N. 2003, *Advances in Space Research*, 31, 869
- Gosling, J. T. 1993, *J. Geophys. Res.*, 98, 18937
- Green, L. M., & Kliem, B. 2009, *ApJ*, 700, L83
- Guo, Y., Ding, M. D., Wiegmann, T., & Li, H. 2008, *ApJ*, 679, 1629
- Hirayama, T. 1974, *Sol. Phys.*, 34, 323
- Howard, R. A., et al. 2008, *Space Sci. Rev.*, 136, 67
- Hundhausen, A. 1999, *The many faces of the sun: a summary of the results from NASA's Solar Maximum Mission.*, 143
- Jing, J., Qiu, J., Lin, J., Qu, M., Xu, Y., & Wang, H. M. 2005, *ApJ*, 620, 1085
- Jing, J., Chen, P. F., Wiegmann, T., Xu, Y., Park, S.-H., & Wang, H. 2009, *ApJ*, 696, 84
- Kahler, S. M. 1992, *ARA&A*, 30, 113
- Kaiser, M. L., et al. 2008, *Space Sci. Rev.*, 136, 5
- Kliem, B., & Török, T. 2006, *Physical Review Letters*, 96, 255002
- Krall, J., Chen, J., Duffin, R. T., Howard, R. A., & Thompson, B. J. 2001, *ApJ*, 562, 1045
- Li, P., Emslie, A. G., & Mariska, J. T. 1993, *ApJ*, 417, 313

- Lin, R. P., et al. 2002, *Sol. Phys.*, 210, 3
- Lin, J., & Forbes, T. G., 2000, *J. Geophys. Res.*, 105, 2375
- Linker, J., Lionello, R., Mikic, Z., & Amari, T. 2001, *J. Geophys. Res.*, 106, 25165
- Liu, C., Lee, J., Yurchyshyn, V., Deng, N., & Cho, K. 2007, *ApJ*, 669, 1372
- Liu, C., & Wang, H. M. 2009, *ApJ*, 696, L27
- MacNeice, P., Antiochos, S. K., Phillips, A., Spicer, D. S., DeVore, C. R., & Olson, K. 2004, *ApJ*, 614, 1028
- Maričić, D. et al. 2007, *Sol. Phys.*, 241, 99
- Martens, P. C., & Zwaan, C. 2001, *ApJ*, 558, 872
- Martin, S. F. 1998, *Sol. Phys.*, 182, 107
- McKenzie, D. E., & Canfield, R. C. 2008, *A&A*, 481, L65
- Moore, R. L., & Labonte, B. J. 1980, *Solar and Interplanetary Dynamics*, 91, 207
- Moore, R. L., Sterling, A. C., Hudson, H. S. & Lemen, J. R. 2001, *ApJ*, 552, 933
- Moore, R. L., & Sterling, A. C. 2006, Washington DC American Geophysical Union Geophysical Monograph Series, 165, 43
- Pick, M., et al. 2006, *Space Science Reviews*, 123, 341
- Poletto, G., & Kopp, R. A. 1986, *The Lower Atmosphere of Solar Flares; Proceedings of the Solar Maximum Mission Symposium*, 453
- Priest, E. R., & Forbes, T.G. 2002, *A&A Rev.*, 10, 313
- Qiu, J., Lee, J., Gary, D. E., & Wang, H. 2002, *ApJ*, 565 1335

- Qiu, J., Wang, H., Cheng, C. Z., & Gary, D. E. 2004, *ApJ*, 604, 900
- Rust, D. M., & LaBonte, B. J. 2005, *ApJ*, 622, L69
- Smart, D. F., & Shea, M. A. 1989, *Journal of Spacecraft and Rockets*, 26, 403
- Scherrer, P. H., et al. 1995, *Sol. Phys.*, 162, 129
- Schrijver, C. J. 2009, *Advances in Space Research*, 43, 739
- Sterling, A. C., Harra, L. K. & Moore, R. L. 2007, *ApJ*, 669, 1359
- Sturrock, P. A. 1989, *Sol. Phys.*, 121, 387
- Sturrock, P. A., Weber, M., Wheatland, M. S., & Wolfson, R. 2001, *ApJ*, 548, 492
- Temmer, M., Veronig, A. M., Vršnak, B., Rybák, J., Gömöry, P., Stoiser, S., & Maričić, D. 2008, *ApJ*, 673, L95
- Thalmann, J. K., & Wiegmann, T. 2008, *A&A*, 484, 495
- Thernisien, A., Vourlidas, A., & Howard, R. A. 2009, *Sol. Phys.*, 256, 111
- Thompson, B. J., Plunkett, S. P., Gurman, J. B., Newmark, J. S., St. Cyr, O. C., & Michels, D. J. 1998, *Geophys. Res. Lett.*, 25, 2465
- Tian, L., Alexander, D., & Nightingale, R. 2008, *ApJ*, 684, 747
- Titov, V. S., Mikic, Z., Linker, J. A., & Lionello, R. 2008, *ApJ*, 675, 1614
- Tripathi, D., Kliem, B., Mason, H. E., Young, P., & Green, L. M. 2009, *ApJ*, 698, L27
- Török, T., & Kliem, B. 2005, *ApJ*, 630, L97
- Vršnak, B., et al. 2004, *Sol. Phys.*, 225, 355

Vršnak, B., & Skender, M. 2005, *Sol. Phys.*, 226, 97

Wang, J. 2006, *Advances in Space Research*, 38, 1887

Webb, D. F., Forbes, T. G., & Aurass, H. et al. 1994, *Sol. Phys.*, 153, 73

Welsch, B. T., DeVore, C. R., & Antiochos, S. K. 2005, *ApJ*, 634, 1395

Wood, B. E., & Howard, R. A. 2009, *ApJ*, 702, 901

Zhang, J., Dere, K. P., Howard, R. A., Kundu, M. R., & White, S. M. 2001, *ApJ*, 559, 452

Zhang, J., Dere, K. P., Howard, R. A. & Vourlidas, A. 2004, *ApJ*, 604, 420

Zhang, J., & Dere, K. P. 2006, *ApJ*, 649, 1100

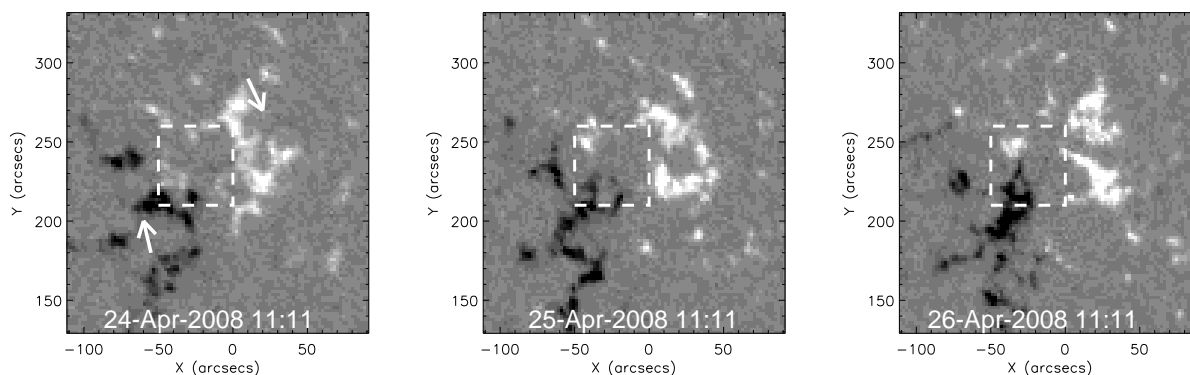


Fig. 1.— Line-of-sight magnetograms with a field of view of  $200'' \times 200''$  taken before the CME eruption. The white square denotes the place of the core field near the PIL, where the main flux cancellation occurred. The two arrows show the motion direction of the two opposite polarities.

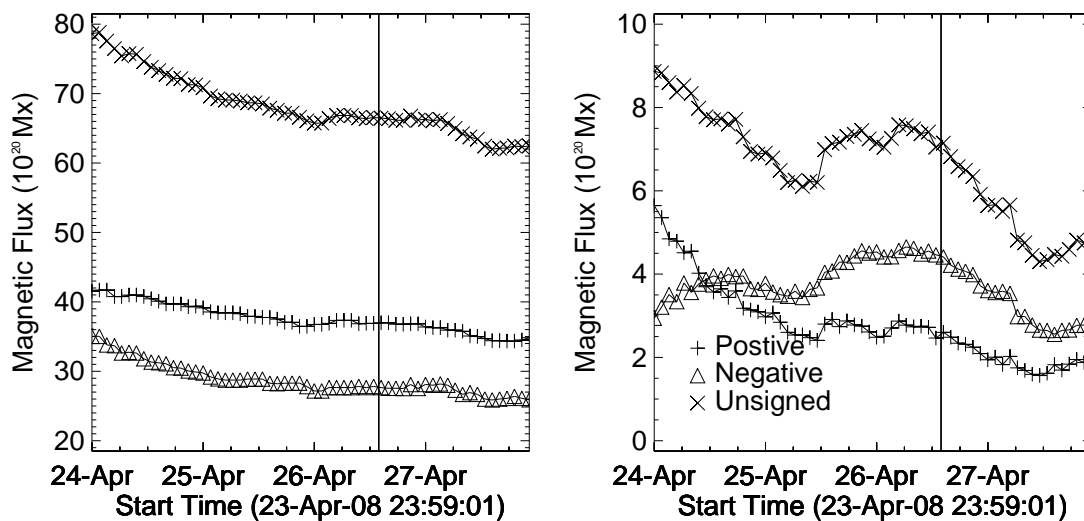


Fig. 2.— The magnetic flux evolution for the whole FOV (left) and that for within the white square (right) in Figure 1. Note that the increase of the negative flux in the right panel is mainly caused by the transportation of negative patch toward northeast. The vertical line denotes the onset of the CME.

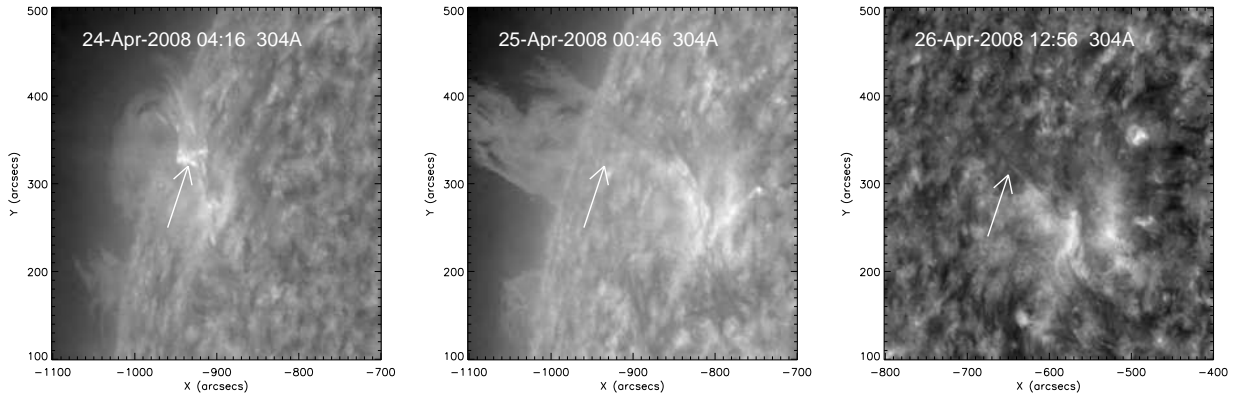


Fig. 3.— EUVI-A 304 Å images showing active filaments and jets before the CME eruption.

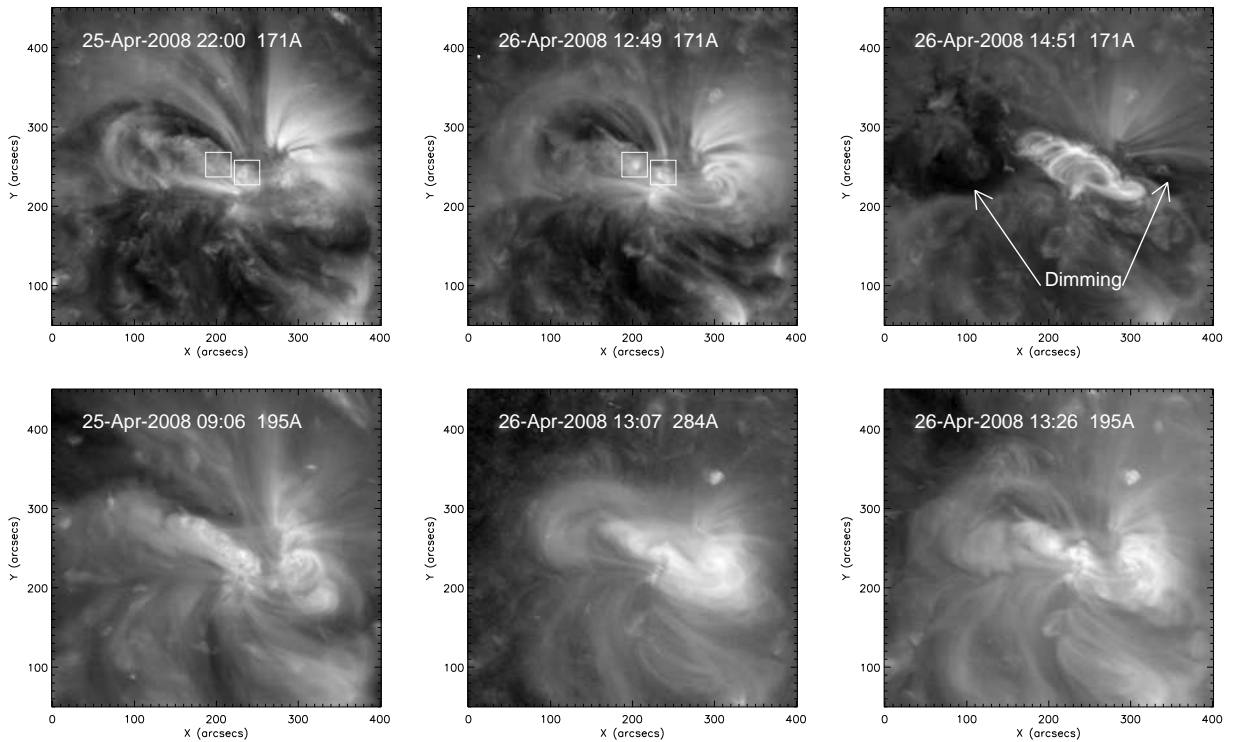


Fig. 4.— EUVI-B images in three different passbands showing the overlying loops and the sigmoid configuration before the CME eruption. The small white squares show the brightening of the core field. The arrows denote the dimming regions.



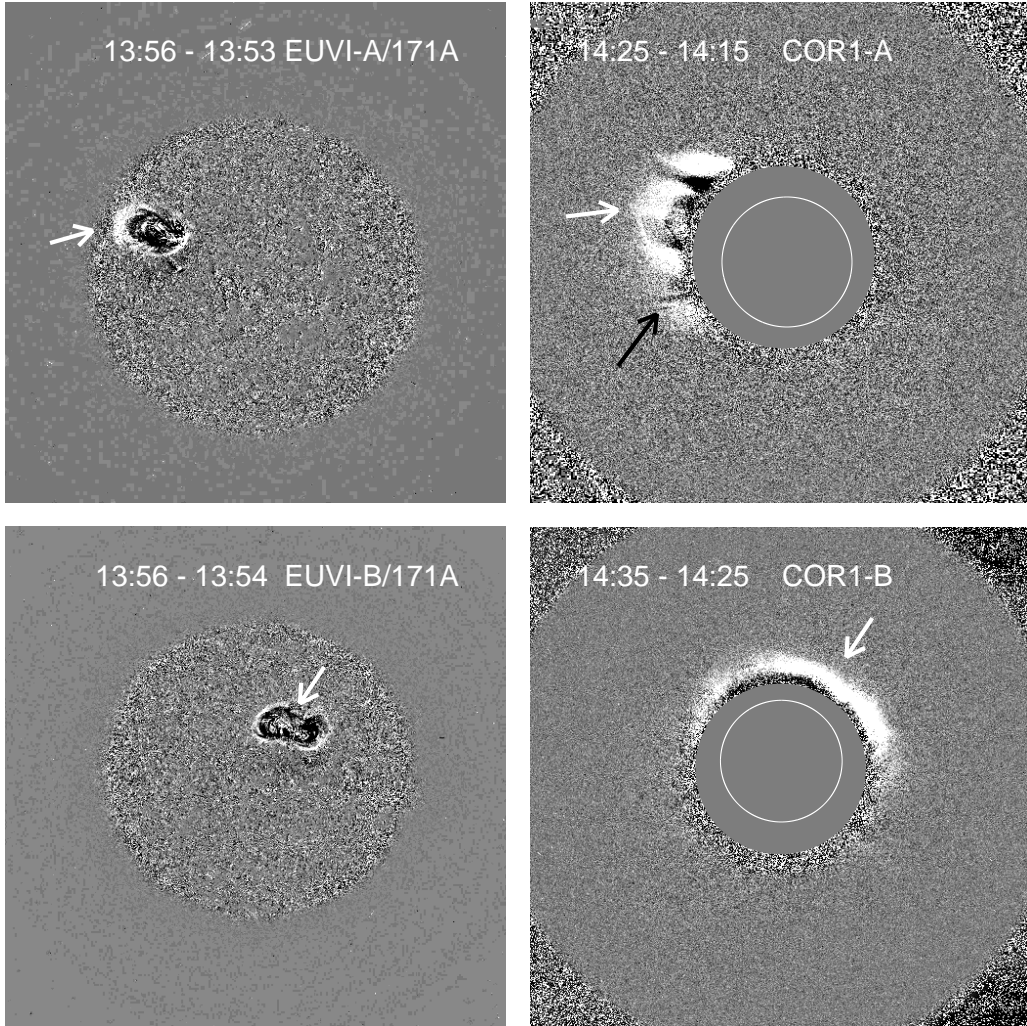


Fig. 5.— STEREO A (top panels) and B (bottom panels) running difference images. The white arrows indicate the CME feature at which we measure the height-time evolution. The black arrow in top-right panel indicates a disturbed streamer.

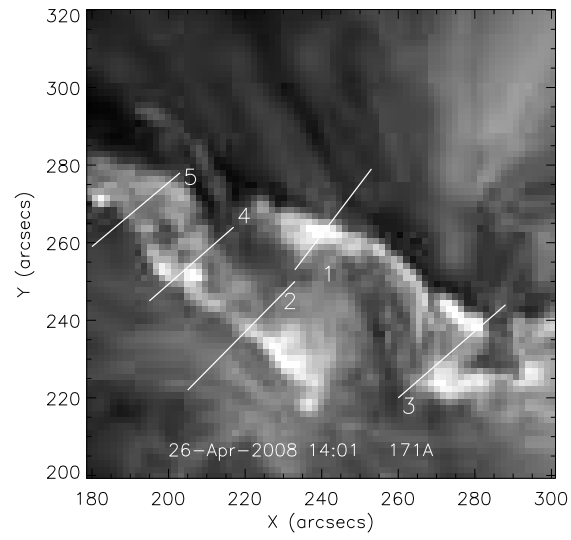


Fig. 6.— An image in 171 Å passband showing flare ribbons. The five lines refer to the directions along which we measure the separation speed of the ribbons.

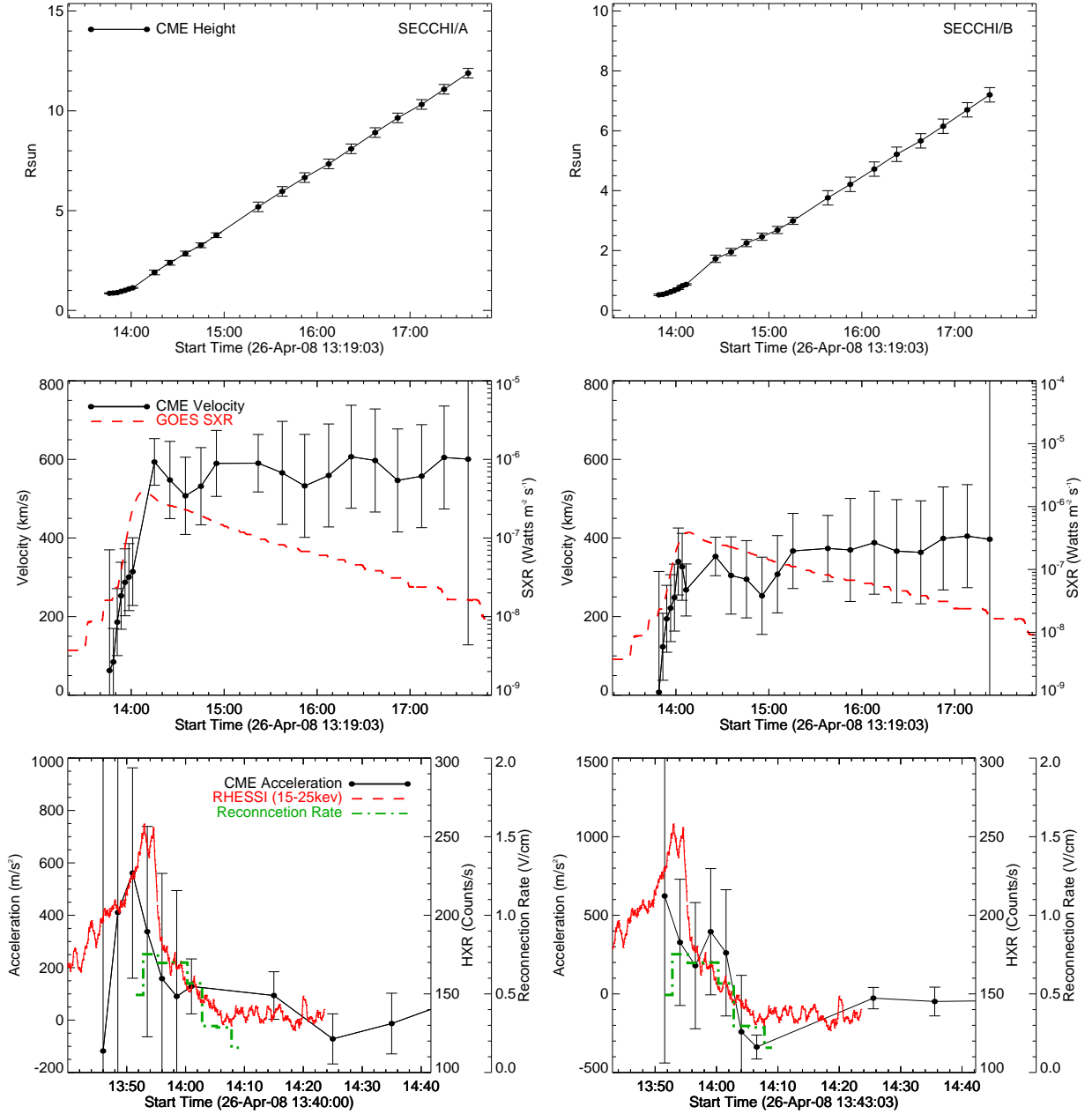


Fig. 7.— The temporal evolution of the height (top), speed (middle), and acceleration (bottom) of the CME obtained from STEREO A (left) and B (right). The GOES SXR and RHESSI HXR flux profiles of the associated flare are shown in the middle panels and the bottom panels, respectively. Also shown in the bottom panels is the reconnection electric field.

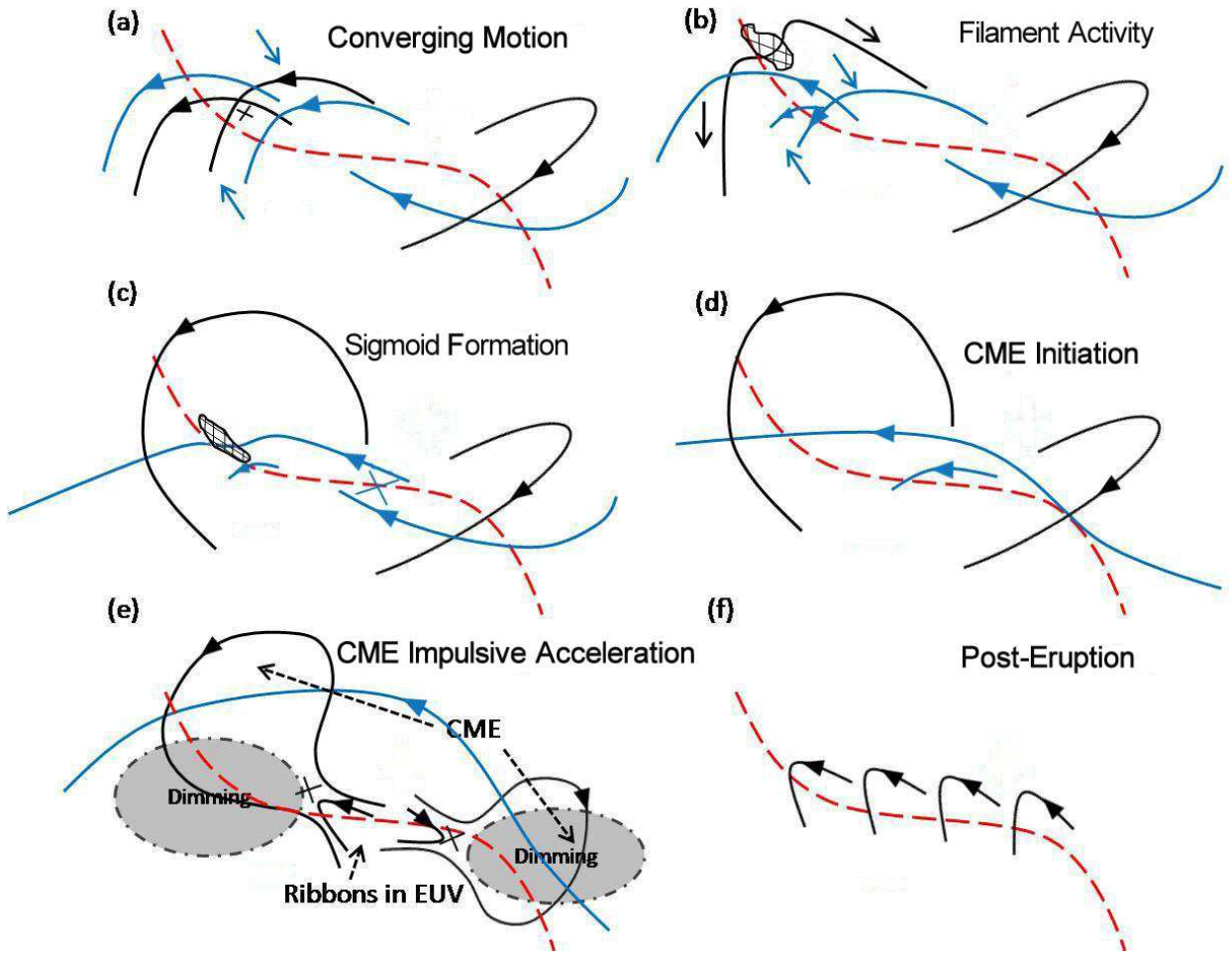


Fig. 8.— A schematic drawing of selected magnetic field lines illustrating the evolution of the event. Black lines refer to the overlying magnetic field and blue lines to the the axis of the flux rope, both of which change obviously in different phases. The red dashed line is the polarity inversion line. The cross denotes the reconnection site.